

## An Application of Linear Programming to Polarimetric Radar Differential Phase Processing

SCOTT E. GIANGRANDE AND ROBERT MCGRAW

*Atmospheric Sciences Division, Brookhaven National Laboratory, Upton, New York*

LEI LEI

*University of Oklahoma, Norman, Oklahoma*

(Manuscript received 11 July 2012, in final form 14 March 2013)

### ABSTRACT

Differential phase and its range derivative  $K_{DP}$  are of interest to several hydrological applications from weather radar systems. Despite the attractive qualities of polarimetric differential phase measurements, the usefulness of these radar measurements is potentially undermined as a consequence of measurement fluctuations and physical or beam geometry artifacts. This paper presents an application of linear programming for physical retrievals, here designed to improve estimates of differential propagation phase by allowing realistic physical constraints of monotonicity and polarimetric radar self-consistency. Results of the linear programming methods to the phase-processing problem are demonstrated at several common weather radar wavelengths (10, 5, and 3 cm).

### 1. Introduction

Detailed microphysical insights from weather radar systems are in demand within operational weather agencies and for the evaluation of numerical weather and climate prediction models, including the construction of model forcing datasets. An emphasis has been on polarimetric radar technology, as highlighted most recently by the upgrade of the U.S. National Weather Service (NWS) Weather Surveillance Radar-1988 Doppler (WSR-88D) network to polarimetric capabilities. Polarimetric systems promise more robust precipitation products over conventional weather radar systems with reduced uncertainty for applications including echo classification, rainfall rate estimation, and drop size distribution (DSD) retrievals.

Hydrological product improvements using polarimetric methods are closely tied to the inclusion of the differential phase  $\Psi_{DP}$  and its range derivative  $K_{DP}$ , which are less sensitive to hail contamination and variation of DSDs, immune to attenuation in rain, radar miscalibration, and

partial beam blockages (e.g., Zrnić and Ryzhkov 1996). Measurements of  $K_{DP}$  as inputs to radar algorithms demonstrate improved accuracy and usefulness of radar rainfall accumulations (e.g., Ryzhkov et al. 2005b; Wang and Chandrasekar 2010; Gourley et al. 2010). The  $K_{DP}$  measurements also allow new opportunities for radar reflectivity factor  $Z$  and differential reflectivity  $Z_{DR}$  quality control and relative calibration monitoring using self-consistency and natural media expectations (intrinsic properties of rain, e.g., Goddard et al. 1994; Scarchilli et al. 1996; Smyth and Illingworth 1998; Bringi and Chandrasekar 2001; Vivekanandan et al. 2003; Ryzhkov et al. 2005a; Giangrande and Ryzhkov 2005).

Despite the attractive qualities of polarimetric phase measurements, the usefulness of propagation differential phase measurements  $\Phi_{DP}$  at operational weather radar wavelengths is lessened as a consequence of measurement noise, unreliability in lighter rainfall and artifacts stemming from nonuniform beam filling (NBF). These NBF artifacts can be associated with the (vertical, horizontal) gradients of  $\Phi_{DP}$  and  $Z$  in the vicinity of stronger convective cells and in response to changes in the vertical profile of reflectivity/differential phase near the melting layer (e.g., Ryzhkov and Zrnić 1998; Ryzhkov 2007). Even if differential phase insights are selectively interjected under advantageous regimes, phase-based rainfall

---

*Corresponding author address:* Scott Giangrande, Atmospheric Sciences Division, Brookhaven National Laboratory, Building 490D, P.O. Box 5000, Upton, NY 11973.  
E-mail: scott.giangrande@bnl.gov

relations commonly demonstrate undesirable characteristics (smearing, speckling) and unphysical behaviors (negative rainfall rates, intrinsic negative behaviors) in the situations of supposed strength (hail and/or melting layer; e.g., Giangrande and Ryzhkov 2008). The challenges are exacerbated at shorter wavelengths, wherein the expectation for an increased (potentially, more reliably sampled) total differential phase shift through similar rain conditions can be compromised by significant contributions from a nonzero differential backscatter phase shift  $\delta$  (herein, we adopt the convention; total measured  $\Psi_{DP} = \Phi_{DP} + \delta$ ). These problems point to the necessity for robust phase-processing methods that attempt to deconvolve propagation  $\Phi_{DP}$  and backscatter  $\delta$  phase components, as these components represent significant independent insights into precipitation microphysics.

Several methods for  $\Psi_{DP}$ ,  $\Phi_{DP}$ , and/or  $K_{DP}$  processing have been proposed to handle challenges associated with the aforementioned issues (e.g., Hubbert et al. 1993; Hubbert and Bringi 1995; Bringi and Chandrasekar 2001; Ryzhkov et al. 2005b; Wang and Chandrasekar 2009; Otto and Russchenberg 2011). To be sure, there is no standard processing or universally adopted approach within the radar community. It is an error to assume existing methods as interchangeable and that processing details do not impact subsequent hydrological products. Recent examples of this sentiment include Cifelli et al. (2011), wherein the National Severe Storms Laboratory (NSSL)  $K_{DP}$  processing and rainfall methods, prototypes for the operational NWS WSR-88D standard, demonstrate functional however nonoptimal performance as compared to methods that include  $K_{DP}$  inputs following Wang and Chandrasekar (2009). As computing power increases, the ease for incorporating additional computational complexity to processing routines should further improve the reliability of fundamental polarimetric phase measurements. For example, several recent studies have already proposed incorporation of polarimetric self-consistency behaviors and realistic physical constraints (e.g., Goddard et al. 1994; Sarchilli et al. 1996) into more complex or nonlinear schemes within research and operational settings (e.g., Otto and Russchenberg 2011; Schneebeli and Berne 2012; Maesaka et al. 2012).

The U.S. Department of Energy (DOE) Atmospheric Radiation Measurement (ARM) Program (Ackerman and Stokes 2003) recently installed several scanning weather radar networks operating at C-band (5 cm) and X-band (3 cm) wavelengths. For these systems, there was immediate demand for open/free source radar processing codes and community data formats that encourage use and visualization of DOE ARM radar datasets. As an

example of an early ARM radar processing activity, this study includes the results for an application of well-known linear programming (LP) concepts (or linear optimization) to the challenge of radar differential phase estimation. This activity was initiated not only as a functional solution to differential phase processing at ARM wavelengths but also as a proof-of-concept motivation for similar physical-based LP retrieval applications in the future. To our knowledge, LP concepts have not been attempted for radar data processing or physical retrievals using radar data, with most LP applications limited to decision making and resource planning in the context of atmospheric sciences (e.g., Helbush 1968; Minciardi et al. 2003). The present study attempts to construct an LP method that shares in the desirable measurement properties sought by existing polarimetric phase-processing techniques, including (i) an ability to maintain monotonic (nonnegative  $K_{DP}$ , e.g., Vivekanandan et al. 2001) behaviors in rain and to isolate  $\Phi_{DP}$  from  $\delta$  contributions (extract a monotonic profile), (ii) producing unbiased  $K_{DP}$  estimates, (iii) adopting polarimetric self-consistency constraints to boost performance in rain regions, and (iv) the potential to resource external datastreams or additional constraints for later improvements. This suggests that our initial methods should share in several benefits of existing nonlinear variational methods that have already been proposed (e.g., Schneebeli and Berne 2012; Maesaka et al. 2012), but herein only a simplified version is offered that is still flexible to handle future modification.

This study is organized as follows. Section 2 describes the linear programming solution to a problem of differential phase processing. Section 3 presents the results of our application of LP methods for a simulated radar dataset at S band (10 cm) and examples collected from the ARM C-band [C-band scanning ARM precipitation radar (CSAPR)] and X-band [X-band scanning ARM precipitation radar (XSAPR)] radar systems in challenging convective storm environments around north-central Oklahoma. Phase processing for this study is benchmarked as compared to NWS WSR-88D phase-processing standards based on NSSL concepts. These results are discussed in section 4 and include additional comments on potential advantages and limitations of LP methods as compared to a wider array of processing options.

## 2. Application of LP to estimate differential propagation phase

This section defines an LP problem associated with polarimetric differential phase processing. Our goal is to demonstrate a reasonable LP retrieval for the  $\Phi_{DP}$  component (having a range derivative  $K_{DP}$ ), which implies

that one may estimate  $\delta$  as a residual of this retrieval and the actual  $\Psi_{DP}$ . For the example LP formulation that follows, a few basic assumptions have been adopted that are similar to many previous processing efforts.

A monotonic behavior is assumed for propagation phase  $\Phi_{DP}$  profiles in rain (nonnegative  $K_{DP}$ ). This assumption should be valid below the melting layer and along radials unaffected by NBF (strong storm or melting layer gradients) or significant artifacts from larger hail (intrinsic negative differential phase behaviors). Invalid data associated with ground clutter, second-trip echo, nonmeteorological, and mixed phase hydrometeors (e.g., melting layer) should be identified so as to adjust (zero out) weighting factors or for possible removal. These problematic gates are identified using polarimetric threshold criteria (often, highly radar specific) for the cross-correlation coefficient  $\rho_{HV}$  or the standard deviation of  $\Psi_{DP}$ . Total  $\Psi_{DP}$  profiles in this LP formulation are also expected unfolded and having nonnegative values.

Profiles of  $\Psi_{DP}$  associated with substantial NBF are challenging for any processing method or eventual  $K_{DP}$  estimation that screens  $\Psi_{DP}$  according to  $\rho_{HV}$  thresholds. While not common, the  $\Psi_{DP}$  profiles in some extreme instances may become too contaminated for accurate differential phase processing. Since  $Z$  fields are less susceptible to NBF (e.g., Ryzhkov 2007), hydrological products in these regions may only be possible using  $Z$ -based or attenuation-based methods.

*a. Minimizing the  $L_1$  norm*

Let  $\mathbf{b} = \{b_1, b_2, \dots, b_n\}$  be the differential phase data array,  $\mathbf{x} = \{x_1, x_2, \dots, x_n\}$  be the variables of the “fit” or processed array, and  $\mathbf{z} = \{z_1, z_2, \dots, z_n\}$  be the variables that appear in the cost function. Each of these arrays is of length  $n$ . To minimize the  $L_1$  norm, we have to minimize

$$L_1 = \sum_{i=1}^n |x_i - b_i|. \tag{1}$$

The standard approach to handle the absolute value (Kiountouzis 1973; Portnoy and Koenker 1997) is to allow either sign possibility for  $x_i - b_i$  by doubling the number of inequality constraints to two for each variable  $x_i$ :

$$\begin{aligned} z_1 &\geq x_1 - b_1; & z_1 &\geq -x_1 + b_1 \\ z_2 &\geq x_2 - b_2; & z_2 &\geq -x_2 + b_2 \\ \dots & & \dots & \\ z_n &\geq x_n - b_n; & z_n &\geq -x_n + b_n \end{aligned} \tag{2}$$

The inequalities in row  $i$  cover the two possibilities: (i)  $x_i - b_i \geq 0$ , in which case  $z_i \geq x_i - b_i = |x_i - b_i|$  and

the second inequality constraint holds trivially (i.e., is inactive) because  $-x_i + b_i$  is either negative or zero; and (ii)  $-x_i + b_i \geq 0$ , in which case  $z_i \geq -x_i + b_i = |x_i - b_i|$  and the first inequality constraint is inactive. In either case, we have  $z_i \geq |x_i - b_i|$  and the minimization of  $L_1$  is equivalent to the minimization of  $n$ -term cost function  $z_1 + z_2 + \dots + z_n$ . This result shows that minimization of the  $L_1$  norm, Eq. (1), can be achieved using LP by doubling the number of inequality constraints and minimizing the cost function:  $z_1 + z_2 + \dots + z_n$ . Note, if inequalities from Eq. (2) are the only constraints in the problem, then the cost function reduces to zero with  $\mathbf{x} = \mathbf{b}$ .

To set up the LP problem in canonical form, we rewrite the left set of inequalities as  $z_i - x_i \geq -b_i$  and the right set as  $z_i + x_i \geq b_i$ , and cast all of these constraints in matrix–vector form as  $\mathbf{Ax}_c \geq \mathbf{b}$ . The  $2n \times 2n$  matrix  $\mathbf{A}$  has block form

$$\mathbf{A} = \begin{pmatrix} \mathbf{I}_n & -\mathbf{I}_n \\ \mathbf{I}_n & \mathbf{I}_n \end{pmatrix}, \tag{3}$$

where  $\mathbf{I}_n$  is the  $n \times n$  identity matrix, and the length  $2n$  vectors  $\mathbf{x}$  and  $\mathbf{b}$  are  $\mathbf{x}_c = \{\mathbf{z}, \mathbf{x}\}^T$ ,  $\mathbf{b} = \{-\mathbf{b}, \mathbf{b}\}^T$ , and the superscript T indicates transpose.

*b. Monotonicity constraint*

For differentiation of discrete and evenly spaced data,  $\mathbf{x} = \{x_1, x_2, \dots, x_n\}$ , we adopt the five-point Savitzky–Golay (SG) second-order polynomial derivative filter [e.g., Madden 1978, Table I, Eq. (III)]:  $\{-0.2, -0.1, 0.0, 0.1, 0.2\}$ . SG least squares convolution filters offer a well-standardized approach to digital data differentiation, with an array of filters of different lengths and orders from which to choose. Reliable  $K_{DP}$  determination requires abstracting reliable derivative estimates from noisy radar data, and in this first presentation of the LP– $K_{DP}$  approach, we limit filter testing to the members from the SG class. The selection of filter length will be discussed later in this section. Monotonicity is enforced through the requirement that the derivative, so defined, be everywhere nonnegative. To avoid edges, the filtering is initiated at the radial position corresponding to  $x_{m+1}$  and ended at  $x_{n-m}$ , where  $2m+1$  is the filter length. Thus, monotonicity according to the five-point filter adds a total of  $n-4$  derivative constraints to the  $2n$   $L_1$  norm minimization constraints already present. The new constraints are

$$\begin{aligned} -0.2x_1 - 0.1x_2 + 0.0x_3 + 0.1x_4 + 0.2x_5 &\geq 0 \\ \dots & \\ -0.2x_{n-4} - 0.1x_{n-3} + 0.0x_{n-2} + 0.1x_{n-1} + 0.2x_n &\geq 0 \end{aligned} \tag{4}$$

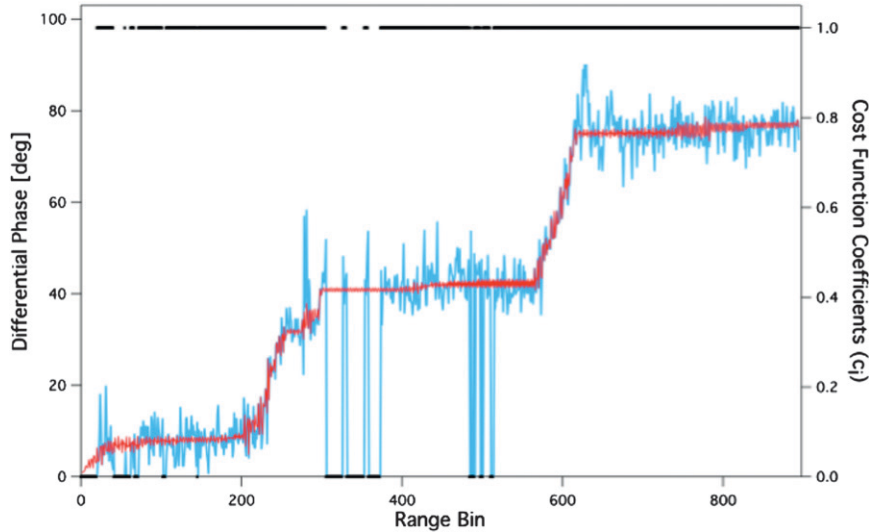


FIG. 1. Comparing measurements of differential phase (blue trace) with the LP-processed result (red trace) along a single radial coordinate. Regions where the differential phase has been set to zero indicate gaps in the measurements. Right axis and black points: Cost function coefficients,  $c_i$ . These coefficients define the cost function, which is minimized in the linear program to obtain the red trace. Note placement of zeros in regions where there are gaps in the measurements, so as to give no weight to these regions in the linear program.

The resulting  $3n - 4 \times 2n$  row augmentation of  $\mathbf{A}$  has the block form

$$\mathbf{A}_{\text{AUG}} = \begin{pmatrix} \mathbf{I}_n & -\mathbf{I}_n \\ \mathbf{I}_n & \mathbf{I}_n \\ \mathbf{Z}_{n-4,n} & \mathbf{M}_{n-4,n} \end{pmatrix}, \quad (5)$$

where  $\mathbf{Z}_{n-4,n}$  is an  $(n - 4) \times n$  matrix of zeros and  $\mathbf{M}_{n-4,n}$  is the like-size matrix of monotonicity constraints. Note from their position in Eq. (5) that inequalities in Eq. (4) operate only on the  $\mathbf{x}$  part of  $\mathbf{x}_c = \{\mathbf{z}, \mathbf{x}\}^T$ . The monotonicity constraints, by themselves, can be written compactly as  $\mathbf{M}_{n-4,n}\mathbf{x} \geq \mathbf{0}$ , where  $\mathbf{x}$  is again of length  $n$ ,  $\mathbf{0}$  is a vector of zeros of length  $n - 4$ , and

$$\mathbf{M}_{n-4,n} = \begin{pmatrix} -0.2 & -0.1 & 0.0 & 0.1 & 0.2 & 0_6 & \dots & 0_n \\ \dots & \dots \\ 0_1 & \dots & 0_{n-5} & -0.2 & -0.1 & 0.0 & 0.1 & 0.2 \end{pmatrix}. \quad (6)$$

Here,  $0_j$  represents a zero in column  $j$ . Vector  $\mathbf{b}$  is also augmented by the addition of 0 to its column, that is, one added zero for each entry on the right-hand side of inequalities in Eq. (4). The totality of constraints is then  $\mathbf{A}_{\text{AUG}}\mathbf{x}_c - \mathbf{b}_{\text{AUG}} \geq \mathbf{0}$ , where  $\mathbf{b}_{\text{AUG}}$  is the augmented version of  $\mathbf{b}$ .

*c. Setting the primal and dual LP problems and their solution*

The solutions of interest are obtained from the following LP problem, here called the primal ( $P$ ) and its dual ( $D$ ):

$$\begin{array}{ll} P: \text{Minimize } \mathbf{c} \cdot \mathbf{x}_c & D: \text{Maximize } \mathbf{w} \cdot \mathbf{b}_{\text{AUG}} \\ \text{subject to } \mathbf{A}_{\text{AUG}}\mathbf{x}_c \geq \mathbf{b}_{\text{AUG}} & \text{subject to } \mathbf{w}\mathbf{A}_{\text{AUG}} \leq \mathbf{c} \\ \mathbf{x}_c \equiv \{\mathbf{z}, \mathbf{x}\}^T \geq \mathbf{0} & \mathbf{w} \geq \mathbf{0} \end{array}$$

The centered dot ( $\cdot$ ) is the dot product. See Bazaraa et al. (2010, chapter 6) for a clear description of the relationship between primal and dual problems in LP. For the primal  $P$ , we require  $\mathbf{z} \geq \mathbf{0}$ , as each of its elements must exceed an absolute value and thus can never be negative. We also require the solution array  $\mathbf{x}$  (differential phase) to be nonnegative, as indicated above. The length  $2n$  vector of cost coefficients,  $\mathbf{c} = \{1_1, \dots, 1_n, 0_{n+1}, \dots, 0_{2n}\}$ , acts in the dot product to sum the elements of  $\mathbf{z}$ , as described above. A useful feature of LP is that  $\mathbf{c}$  is easily modified to handle a nonuniform distribution of weights. Figure 1 shows an arbitrary radial of 5-cm CSAPR data with gaps (blue trace). Here, the cost function was modified by setting unit weights to zero in regions of “missing” data so as to give zero weight to those regions. Modified cost coefficients  $1 - n$  are indicated by the black dots in Fig. 1.

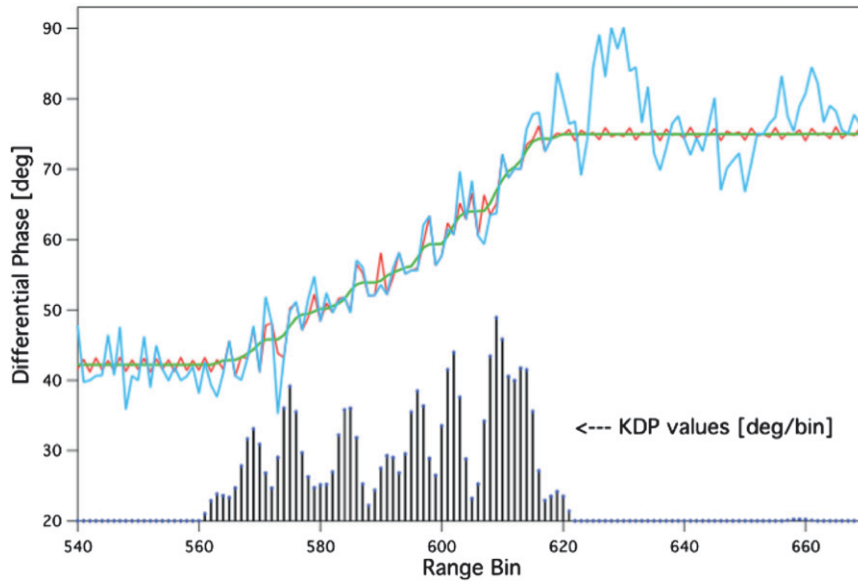


FIG. 2. Blowup of range 600 region from Fig. 1 showing original measurements of differential phase (blue curve) together with the LP-processed result (red curve), and result (green curve) of applying the five-point smoothing filter to the red curve. Values of  $K_{DP}$  (degrees per range bin), as evaluated by applying the five-point derivative filter to the green curve, are also shown. For display purposes, the  $K_{DP}$  trace has been shifted vertically with the baseline (originally at 0) now at 20 and amplitude (vertical scale) expanded by a factor of 20 for clarity.

The red trace in the figure marks the optimal solution for  $\mathbf{x}$  from problem  $P$ . One immediately notices a significant level of noise reduction compared to the original data (blue trace). The modified cost function allows the optimal LP solution to match the original data across gaps without penalty. Another important property of the optimal solution is that it is “global,” in the sense that it is computed at once for the entire radial trace. This global property makes the LP optimized solution less pervious to local variations in the data, like the substantial peak just beyond the range bin of 600 most likely associated with  $\delta$ .

For the problems we have examined, both  $P$  and  $D$  have optimal solutions that can be generated simultaneously using the simplex method (see below). The fundamental theorem of linear programming then states these must have equal objectives (i.e.,  $\mathbf{c} \cdot \mathbf{x}_c = \mathbf{w} \cdot \mathbf{b}_{AUG}$ )—that is, the minimum cost solution for problem  $P$  maximizes the objective for problem  $D$  (Bazaraa et al. 2010, chapter 6). This minimax property provides a quick check on whether an optimal solution has been found. The array elements of  $\mathbf{w}$  also provide cost sensitivities to changes in the constraints of  $P$ . These and other useful properties of the dual form can be explored in future studies.

#### d. Derivative and smoothing filters

Length  $L = 2m + 1$  SG derivative filters applied in this study are antisymmetric filters of the form

$$\mathbf{d}_n = \{d_{-m}, d_{-m+1}, \dots, d_{-1}, d_0, d_1, \dots, d_{m-1}, d_m\}. \quad (7)$$

Properties of these filters that we will require later are (Madden 1978)

$$\begin{aligned} \sum_{i=-m}^m d_i &= 0 \\ \sum_{i=-m}^m i d_i &= 1. \end{aligned} \quad (8)$$

In applying LP to the analysis of radar data, we require of the optimized solution that it satisfy the nonnegativity constraints

$$\begin{aligned} D(i) &= d_m x(i+m) + d_{m-1} x(i+m-1) + \dots + d_0 x(i) \\ &+ d_{-1} x(i-1) + \dots + d_{-m} x(i-m) \geq 0 \end{aligned} \quad (9)$$

for all  $i$ . Even with these constraints in place, however, the processed signal can still oscillate (see, e.g., the red traces in Figs. 1 and 2). To understand what is happening, consider the simple three-point filter  $\mathbf{d}_3 = \{-0.5, 0.0, 0.5\}$ . For this case the inequalities in Eq. (9) require only that the odd-numbered element and even-numbered element subsequences of  $\mathbf{x}$  be separately monotonic. There is no

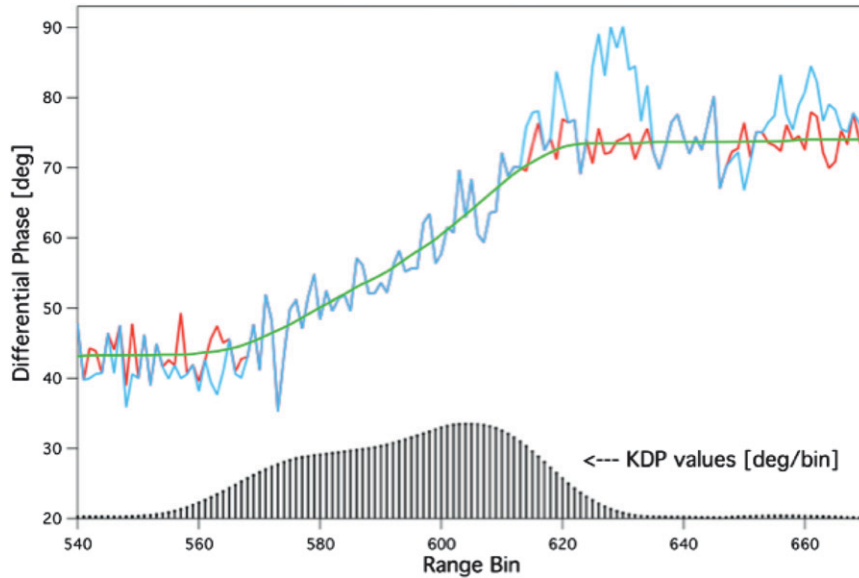


FIG. 3. As in Fig. 2, but showing the LP-processed result (red curve) obtained using non-negative derivative constraints based on the 25-point derivative filter in the linear program, and result (green curve) of applying the corresponding 25-point smoothing filter to the red curve.

requirement that neighboring differences,  $x(i + 1) - x(i)$ , be nonnegative. In other words, the processed signal can still oscillate so long as  $x(i + 2) - x(i) \geq 0$  for  $i$  when it is even or odd. Figure 2 shows similar oscillations resulting from the five-point filter LP solution more clearly in an expanded version of Fig. 1 (red trace). Indeed, the LP solution to  $L_1$  norm minimization makes use of such oscillations as it tries to match noise present in the original data so as to minimize the cost function. We will refer to an LP-optimized signal that satisfies constraints  $D(i) \geq 0$  for all  $i$  as being “weakly monotonic.” Although its filter derivative is strictly nonnegative, such a weakly monotonic trace can still exhibit oscillations on scales shorter than the filter length.

For any filter, filter width should be roughly twice the full width at half height of the smallest feature one is attempting to resolve (Enke and Nieman 1976). For the typical operational and ARM weather radar gate spacing of  $\sim 100$  m, this implies that a five-point filter is attempting to resolve features larger than 0.5 km. Longer derivative filters in the LP allow more leeway for oscillation; instead of smoothing the optimized solution, more oscillations manifest at subfilter-length scales with an increase in filter length. Figure 3 shows results from using the 25-point derivative filter from Madden [1978, Table I, Eq. (III)] for  $m = 12$ . Notice in the gradually increasing region of differential phase, oscillations in the optimized trace (red) track noise fluctuations in the measurements (blue) almost perfectly. In this region, the derivative

constraints tend to be inactive (the derivative is positive anyway), allowing  $L_1$  minimization to take over. Elements of the dual solution vector  $\mathbf{w}$  tend to be zero in this region as well—illustrating a well-known property of the primal–dual relationship known in LP as the complementary slackness condition.

Fortunately, these subfilter-length oscillations can be eliminated completely in a single postprocessing step with the appropriate smoothing filter. For each SG derivative filter, there is a uniquely defined smoothing filter having the same length. For example, for  $\mathbf{d}_3$  defined as above, the smoothing filter is  $\mathbf{s}_3 = \{0.25, 0.5, 0.25\}$ . We now obtain these smoothing filters for the general case:

$$\mathbf{s}_n = \{s_{-m}, s_{-m+1}, \dots, s_{-1}, s_0, s_1, \dots, s_{m-1}, s_m\}. \tag{10}$$

Consider the action of  $\mathbf{s}_n$  on two adjacent subsequences from the LP-processed sequence  $\mathbf{x}$ :

$$\begin{aligned} S(i) &= s_m x(i + m) + s_{m-1} x(i + m - 1) + \dots + s_0 x(i) \\ &\quad + s_{-1} x(i - 1) + \dots + s_{-m} x(i - m) \\ S(i + 1) &= s_m x(i + m + 1) + s_{m-1} x(i + m) + \dots + s_0 x(i + 1) \\ &\quad + s_{-1} x(i) + \dots + s_{-m} x(i - m + 1). \end{aligned} \tag{11}$$

We obtain the smoothing coefficients  $\{s_i\}$  from the derivative filter coefficients  $\{d_i\}$  using the condition

$$\begin{aligned}
S(i+1) - S(i) &= s_m[x(i+m+1) - x(i+m)] + \cdots + s_0[x(i+1) - x(i)] + \cdots + s_{-m}[x(i-m+1) - x(i-m)] \\
&= \frac{1}{2} \left\{ [d_m x(i+m) + d_{m-1} x(i+m-1) + \cdots + 0x(i) + d_{-1} x(i-1) + \cdots + d_{-m} x(i-m)] + \right. \\
&\quad \left. [d_m x(i+m+1) + d_{m-1} x(i+m) + \cdots + 0x(i+1) + d_{-1} x(i) + \cdots + d_{-m} x(i-m+1)] \right\} \\
&= \frac{1}{2} [D(i) + D(i+1)] \geq 0, \tag{12}
\end{aligned}$$

where the final inequality from Eq. (12) is the starting point and follows from the inequality listed in Eq. (9), and is a simple weighting of the derivatives evaluated at the endpoints of the interval under consideration. Equating coefficients for each of the  $x(i)$  and back substitution gives

$$\begin{aligned}
s_m &= d_m/2 \\
s_{m-1} &= d_m + d_{m-1}/2 \\
s_{m-2} &= d_m + d_{m-1} + d_{m-2}/2 \\
&\quad \cdots \\
s_1 &= d_m + d_{m-1} + \cdots + d_2 + d_1/2 \\
s_0 &= d_m + d_{m-1} + \cdots + d_2 + d_1 + d_0/2 \\
&= -d_{-m} - d_{-m+1} - \cdots - d_{-2} - d_{-1} - d_0/2 \\
s_{-1} &= -d_{-m} - d_{-m+1} - \cdots - d_{-2} - d_{-1}/2 \\
&\quad \cdots \\
s_{-m+1} &= -d_{-m} - d_{-m+1}/2 \\
s_{-m} &= -d_{-m}/2. \tag{13}
\end{aligned}$$

The second equality of  $s_0$  makes use of the first property of Eq. (8). Finally, it is not difficult to show from Eq. (13) and the second property of Eq. (8) that the sum of the  $n$  smoothing filter coefficients is unity:

$$\sum_{i=-m}^m s_i = 1. \tag{14}$$

The smoothing filters developed here are very similar to the standard SG smoothing filters (Madden 1978). They have the same normalization and same shape, which is parabolic for the second-order polynomial cases we show, but they are somewhat broader and shortened in vertical extent. Differences are to be expected, as the standard SG smoothers are defined to operate at a single discrete point, located at the center of the filter, whereas ours [cf. Eq. (12)] involves differences and averaging over an interval of two neighboring points.

For the five-point derivative filter used in this study,  $d_2 = 0.2$ ,  $d_1 = 0.1$ ,  $d_0 = 0$ ,  $d_{-1} = -0.1$ , and  $d_{-2} = -0.2$ . Substitution into Eq. (13) gives the corresponding smoothing filter corresponding to  $\mathbf{d}_5$  as  $\mathbf{s}_5 = \{0.1, 0.25,$

$0.3, 0.25, 0.1\}$ . The green trace of Fig. 2 results from applying this smoothing filter to the red trace (LP solution) and shows complete removal of the oscillations. We will refer to the smoothed trace as exhibiting a “strong monotonicity” condition, whereby monotonicity is preserved at all scales down to the smallest scale of the data spacing.

Figure 2 also shows the result of applying the derivative filter  $\mathbf{d}_5$  to the smoothed green trace, thereby smoothing the derivative by removing the influence of noise-matching oscillations in the LP derivative in the same way that the smoothing filter removes these oscillations from  $x(i)$ . Smoothing, as a postprocessing step applied to the LP solution, allows the benefits of using longer derivative and smoothing filters to be realized. Figure 3 shows similar results for the 25-point filter. Again, Eqs. (13) have been used to develop a smoothing filter,  $\mathbf{s}_{25}$ , that when applied to the weakly monotonic red trace yields the strongly monotonic green one. Application of  $\mathbf{d}_{25}$  to the green trace yields the correspondingly smoothed derivative field. Note that these derivatives are proportional to (since the range bins are arbitrary length)  $K_{DP}$  in degrees per kilometer.

#### e. Self-consistency constraints

One adjustment to improve performance of the optimal LP solution is to incorporate additional physical (or radar self-consistency) constraints. We introduce one modification here—that is, to modify the right-hand-side constraints in  $P$ :  $\mathbf{b} \geq 0$ . These constraints ensure monotonicity, but it follows that modified values may interject additional insights from reliable polarimetric radar fields to reinforce whether derivatives ( $K_{DP}$ ) receive additional nonzero behaviors ( $\mathbf{b} \geq$  a positive nonzero value). We suggest a “steering” of  $K_{DP}$  in a self-consistent manner associated with locations of higher  $Z$ , as in a form  $b_i \geq K_{DP}(Z_i) = aZ^b$ . Here, the power-law coefficients can be modified to provide only weak constraints, or to better match theoretical expectations. Steering with additional weighting factors was found to quickly improve  $K_{DP}$  field behaviors to more closely resemble only those cell patterns found in  $Z$  or to ignore low  $Z$  regions also having low cross-correlation coefficient  $\rho_{HV}$  (e.g., redundancy checks for insects, ground

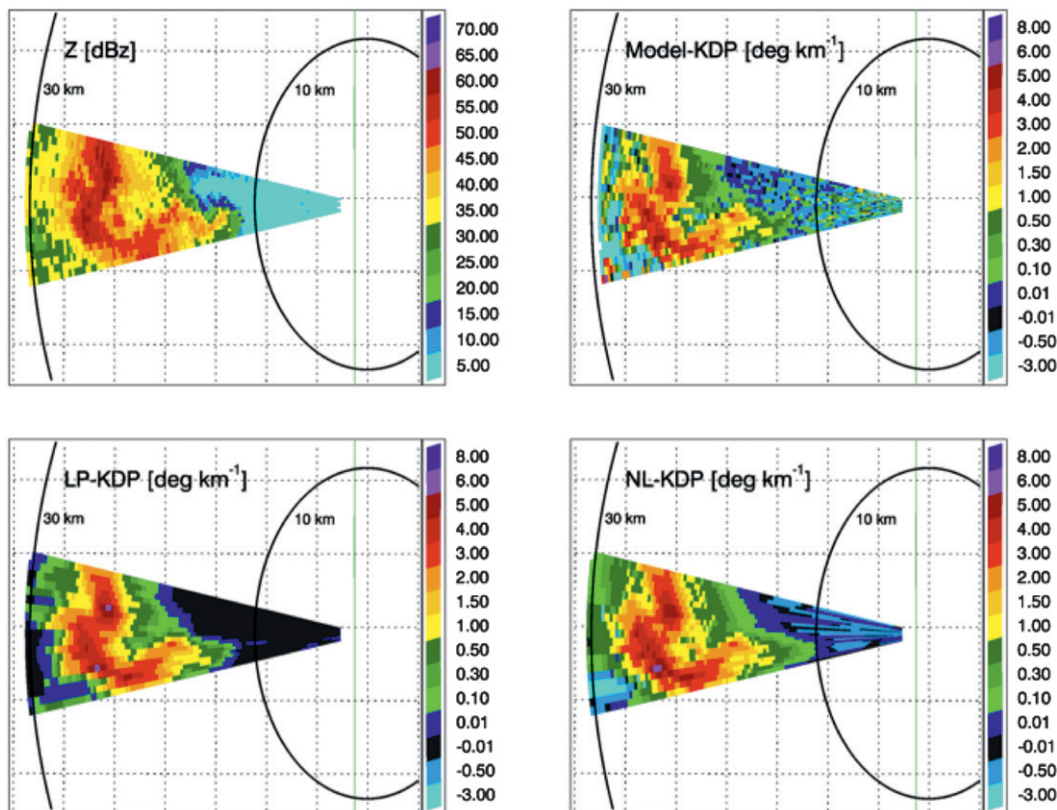


FIG. 4. PPI images at S-band wavelength (10 cm) for simulated fields of  $Z$  and  $K_{DP}$ , as well as subsequent processing of  $K_{DP}$  from LP and NL methods.

clutter echo). At shorter wavelengths and as a consequence of attenuation in rain,  $Z$  fields may also require additional processing to include a baseline linear correction for attenuation in rain that capitalizes on a first-pass heavily smoothed differential phase profile (or iterative processing). Note that in situations having possible hail/mixed phase contamination, care must be taken to mitigate the associated influence on  $Z$  measurements (e.g.,  $Z$  threshold/cap). Here, we suggest the influence weighting of  $Z$  may be capped at 50–53 dBZ for the possible presence of hail.

#### f. Solutions for the LP problem and computational considerations

Numerical solutions to the LP problem are obtained using the simplex method of Dantzig (1963). These methods are available in many popular software packages and within the open/free source community. Recent algorithmic approaches to LP, including interior point methods (e.g., Bazaraa et al. 2010, chapter 8; Portnoy and Koenker 1997), known to greatly improve computational speed for certain types of problems, were not tested for their computational speed at the time of this writing. It is also noted that computational speed for numerical

solutions to LP problems, including the simplex method, is contingent on the number of points in the data arrays. Computational speed behavior was found superlinear for this study. An ability to perform data array reduction (or applications on shorter-wavelength systems that typically imply fewer range gates) can greatly reduce computational time. Parallelization is an option for the processing of LP methods as described, since all operations are performed along single radial arrays.

### 3. Results

In this section, we provide CSAPR and XSAPR radar observations following LP- $K_{DP}$  estimation (LP -  $K_{DP}$ ) as compared to observed polarimetric fields and  $K_{DP}$  processing following NSSL-type smoothing methodology (NL -  $K_{DP}$ , e.g., Ryzhkov et al. 2005b). The ARM radars provide an interesting challenge since X- and C-band datasets exhibit strong convective storm cores with potential  $\delta$  behaviors not observed at operational NWS WSR-88D wavelengths. Since NSSL methods were not originally intended for application at shorter ARM wavelengths, the authors have attempted to faithfully adjust these methods and associated thresholds for the

ARM systems. The particular ARM radar systems for use in this study are located near Lamont, Oklahoma. ARM radars feature radar gate spacing of approximately 100 m and a beamwidth of  $1^\circ$ . Although advanced clutter suppression is planned for the ARM radar systems (e.g., Bharadwaj et al. 2010), existing ARM datasets require additional processing to identify echoes contaminated with insect and ground clutter from hydrometeor-linked differential phase measurements. This is accomplished using simple cutoffs to avoid regions having a lower cross-correlation coefficient and higher along-radial standard deviations of differential phase (e.g., Wang and Chandrasekar 2009). For the ARM X-band radar systems at the time of this study, the data quality was found at the lower end of research-quality standards as compared to previous differential phase measurement expectations at X band (e.g., Park et al. 2005; Matrosov et al. 2006).

The results of a simulated convective storm radar dataset at S band (10 cm) are also included to further evaluate the performance of the LP- $K_{DP}$  and NL- $K_{DP}$  methods. Here, simulated radar fields provide an opportunity to test the LP formulation under ideal but NWS operationally relevant conditions. At these wavelengths, we will assume  $\Psi_{DP}$  is associated only with  $\Phi_{DP}$  and fluctuation noise, having  $\delta = 0$ . The simulator does not account for profile behaviors associated with NBF, as has been previously discussed at S band by Ryzhkov and Zrnić (1998). The radar simulator is based on Advanced Regional Prediction System (ARPS) model outputs (Xue et al. 2000; Jung et al. 2008a,b) having a conventional radar emulation for a thunderstorm simulation as viewed at radar grazing angles and previously outlined in Cheong et al. (2008). The simulation capitalizes on Kessler-type warm rain microphysics (exponential DSD assumption) for a 20 May 1997 Del City, Oklahoma, sounding environment [as from Ray et al. (1981)] with the radar simulator expanded to include realistic polarimetric fields at S band following Lei et al. (2009).

#### a. Performance with simulated storm outputs

Figure 4 includes simulated plan position indicator (PPI) images of the model output  $Z$  field, as well as a  $K_{DP}$  from the intrinsic radar model output, the NSSL-based and LP-based processing methodologies. Because the radar model outputs a  $K_{DP}$  field that may be considered a “truth” field, we have separately plotted the scatterplot of the LP- $K_{DP}$  and NL- $K_{DP}$  performances as compared to model truth  $K_{DP}$  values (Fig. 5). Note that from these S-band model examples,  $K_{DP}$  values at maximum are allowed to approach  $7^\circ \text{ km}^{-1}$  having  $Z$  exceeding 60 dBZ. From PPI imagery in Fig. 4, all  $K_{DP}$  fields typically demonstrate desirable (nonnegative)

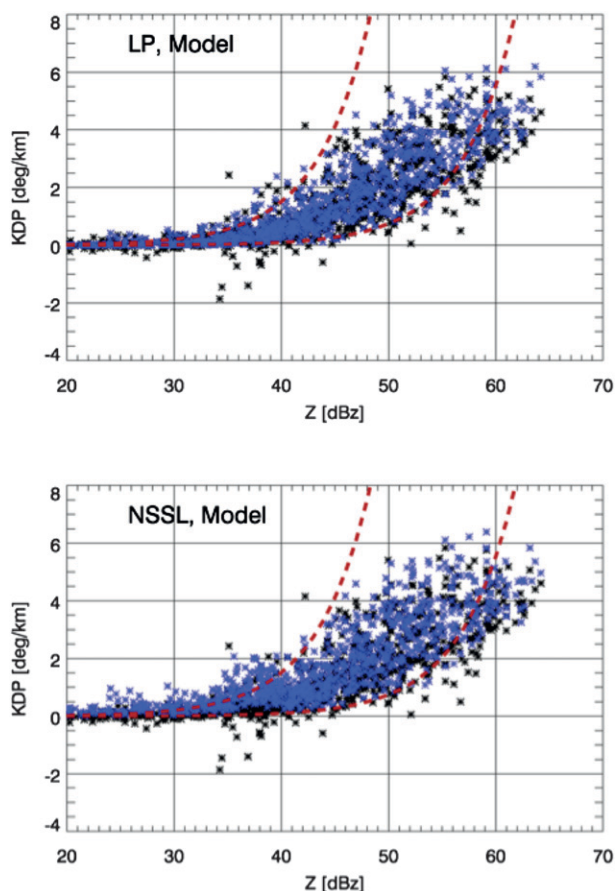


FIG. 5. Scatterplot of  $Z$  vs LP and NSSL(NL)-processed  $K_{DP}$  fields (blue) as compared to model-simulated  $K_{DP}$  fields for simulation as in Fig. 4. Red dashed curves are provided only as additional reference lines.

results that match storm hook echolike behavior found in the  $Z$  field. This result is not surprising, since NBF is not allowed in our model and  $\delta$  is negligible. Thus, fluctuation noise in  $\Psi_{DP}$  tends to be readily removed with smoothing for simulation fields and in regions of high  $Z$ . Negative  $K_{DP}$  data regions after processing are limited and located only at the periphery of the convective cell in low  $Z$  regions.

The suggested LP-based method enforces nonnegative  $K_{DP}$ . For such nonnegative  $K_{DP}$  fields, there was a concern of possible positive bias that might have been inadvertently interjected to ensure this behavior. Scatterplots in Fig. 5 reflect that there is no significant mean bias found between the processed  $K_{DP}$  fields. For regions of  $Z > 40$  dBZ, the mean bias between the model and LP- $K_{DP}$  field is found to be  $0.1^\circ \text{ km}^{-1}$  (overestimate). NSSL methods for  $Z > 40$  dBZ reflect a negative smoothing and  $K_{DP}$  calculation procedure (assumed slightly more smeared than LP efforts), exhibits a  $0.18^\circ \text{ km}^{-1}$  mean bias (overestimate). For typical values

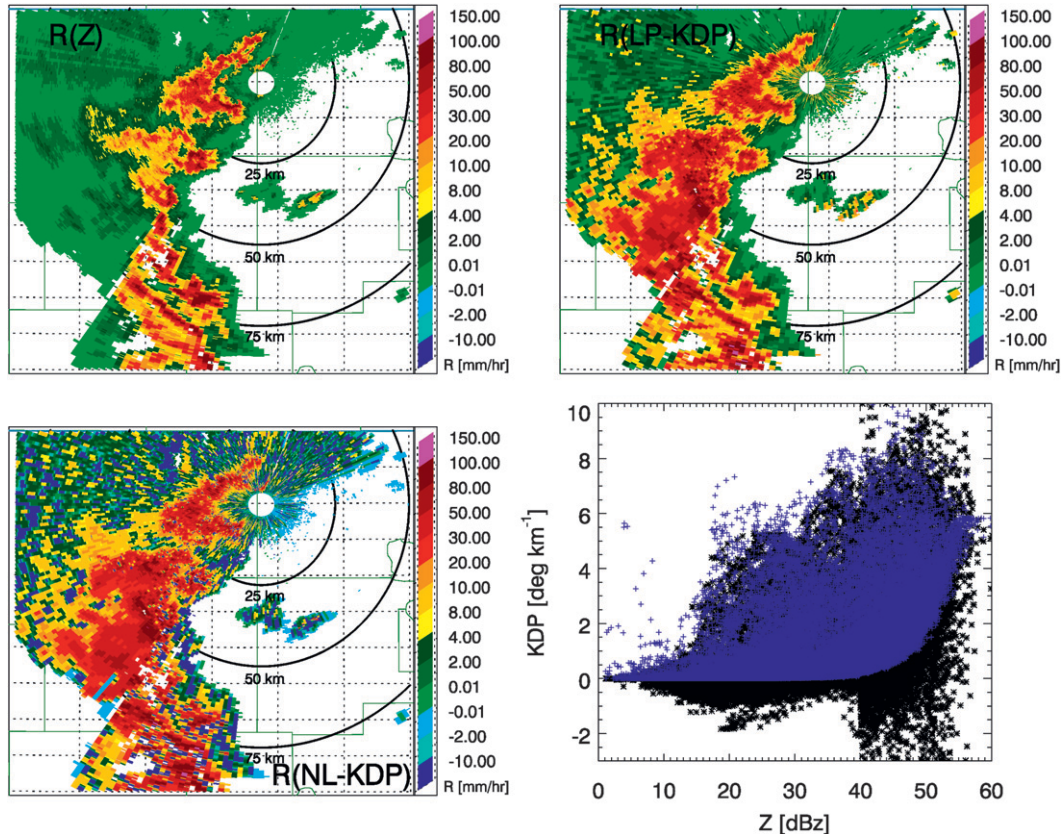


FIG. 6. PPI images of rainfall rates as calculated at C-band wavelength (5 cm) for  $R(Z)$ ,  $R(LP-K_{DP})$ , and  $R(NL-K_{DP})$ . Scatterplot contains the  $Z$  vs  $K_{DP}$  behaviors associated with the rainfall rate fields. Event is from the CSAPR radar on 20 May 2011.

of  $K_{DP}$  for that interval of  $Z$ , this relative error is to within 10%. The most visible discrepancy between the methods occurs at  $Z < 40$  dBZ, where it should be stated that the NSSL  $K_{DP}$  is processed using a longer smoothing window (25 gates) and  $K_{DP}$  is generally assumed less reliable for operational radar applications at S band. Note that the standard deviations of the LP- $K_{DP}$  and NL- $K_{DP}$  results are improved as compared to the  $K_{DP}$  field from the simulator, but especially in the case of the LP method. These results support an initial goal of this study to suggest LP methods as suitable for radar phase processing without imposing a bias.

#### b. Performance on observed ARM radar datasets

Figures 6 and 7 include plots of rainfall rates  $R(Z)$ ,  $R(NL-K_{DP})$ ,  $R(LP-K_{DP})$  and scatterplots of  $K_{DP}$  versus  $Z$  for events viewed by the CSAPR (Fig. 6) and XSAPR (Fig. 7) radar systems, respectively. The  $R$  operation denotes that  $Z$  and  $K_{DP}$  values have been converted to rainfall rate fields ( $\text{mm h}^{-1}$ ) for ease in cross comparisons between the panel images. Rainfall relation operators follow standard rainfall and Oklahoma-specific relations

found in the literature (e.g., Bringi and Chandrasekar 2001; Gu et al. 2011). For the CSAPR, we use a matched Oklahoma rainfall rate  $R(K_{DP})$  expression:

$$R(K_{DP}) = 25.1 \times K_{DP}^{0.777} \text{ (mm h}^{-1}\text{)}, \quad (15)$$

and for the XSAPR,

$$R(K_{DP}) = 16.9 \times K_{DP}^{0.801} \text{ (mm h}^{-1}\text{)}. \quad (16)$$

Note, the NSSL-based  $K_{DP}$  estimates may be negative as a consequence of fixed radial smoothing windows and these situations are handled by associating the negative  $K_{DP}$  values with negative rainfall rates comparable to positive counterparts (e.g., Ryzhkov et al. 2005a,b). For these plots,  $Z$  has been corrected for attenuation in rain following the methods of Gu et al. (2011) and using the LP-processed differential phase profiles.

Figure 6 highlights an impressive squall-line event that developed over north-central Oklahoma on 20 May 2011, with values of accumulated  $\Psi_{DP}$  exceeding  $300^\circ$  along several radials prior to complete extinction (Fig. 8).

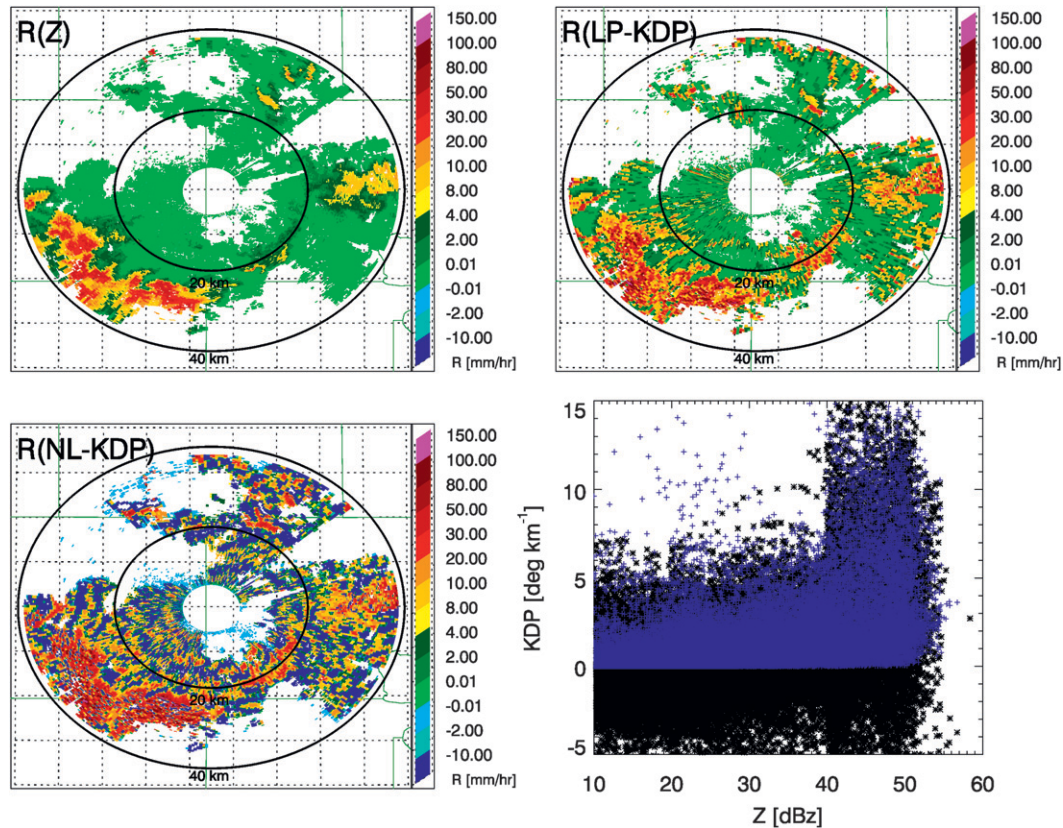


FIG. 7. As in Fig. 6, but for the 23 May 2011 event from the southeast XSAPR (3-cm wavelength) system.

Figure 7 illustrates an isolated severe convective event that took place on 23 May 2011 and includes several storms meeting NWS severe thunderstorm criteria for significant hail ( $>2$  cm) and tornadic activity. Associated differential phase and  $Z$  radials for Fig. 7 are located in Fig. 9.

As in the previous simulated radar dataset convective example at S band, there is an apparent significant benefit for the CSAPR and XSAPR datasets when switching to the LP- $K_{DP}$  formulation as compared to NL- $K_{DP}$ . It should be noted that both  $K_{DP}$ -based fields from the CSAPR event in Fig. 6 offer significant value for rainfall estimation with noticeably attenuated regions for  $Z$  behind the squall line. Note that scatterplot behaviors in Figs. 6 and 7 still imply  $Z$  attenuation corrections did not always completely recover these fields.

The performance of  $R(LP-K_{DP})$  is significantly cleaner for the XSAPR examples in Fig. 7 and in associated  $\Phi_{DP}$  profile retrievals as in Fig. 9, where the greatest benefit to these methods is argued. The 23 May 2011 event was a significant convective storm outbreak example with hail contamination (suggested also by radials in Fig. 9 featuring cores exceeding 55–60 dBZ). In addition to larger  $\delta$  contributions near strong cores,

extended nonmonotonic  $\Psi_{DP}$  behaviors are more frequently observed at X band, as NBF is proportional to the gradients of differential phase (e.g., Ryzhkov 2007). We suggest that the oscillations of  $\Psi_{DP}$  associated with fluctuation noise, NBF, and  $\delta$  in the vicinity of these convective cells are not as well handled by the fixed NSSL smoothing procedures that also attempt to rely on a  $\rho_{HV}$  threshold to isolate and/or interpolate over exceptionally problematic/hail regions. This is a particularly challenging case, since the low  $\rho_{HV} \sim 0.9$  threshold is not sufficient to properly identify NBF- and/or  $\delta$ -prone regions. From Fig. 7, NL- $K_{DP}$  and associated  $R(NL-K_{DP})$  fields are shown in reasonable agreement for high  $Z > 40$  dBZ regions having stronger polarimetric phase measurement contrasts. However, these regions exhibit extended negative  $K_{DP}$  regions (decreasing estimated  $\Phi_{DP}$  along radials for several kilometers) in regions having  $Z > 40$  dBZ that are apparently better handled by LP- $K_{DP}$  method examples. Profile slopes from the offered LP formulation through stronger storm core regions (Fig. 9) are consistent and typically do not exceed  $7^{\circ}$ – $10^{\circ} \text{ km}^{-1}$ . These slopes correspond to rainfall rates on the order of  $70$ – $100 \text{ mm h}^{-1}$  at XSAPR using the expressions such as in Eq. (16).

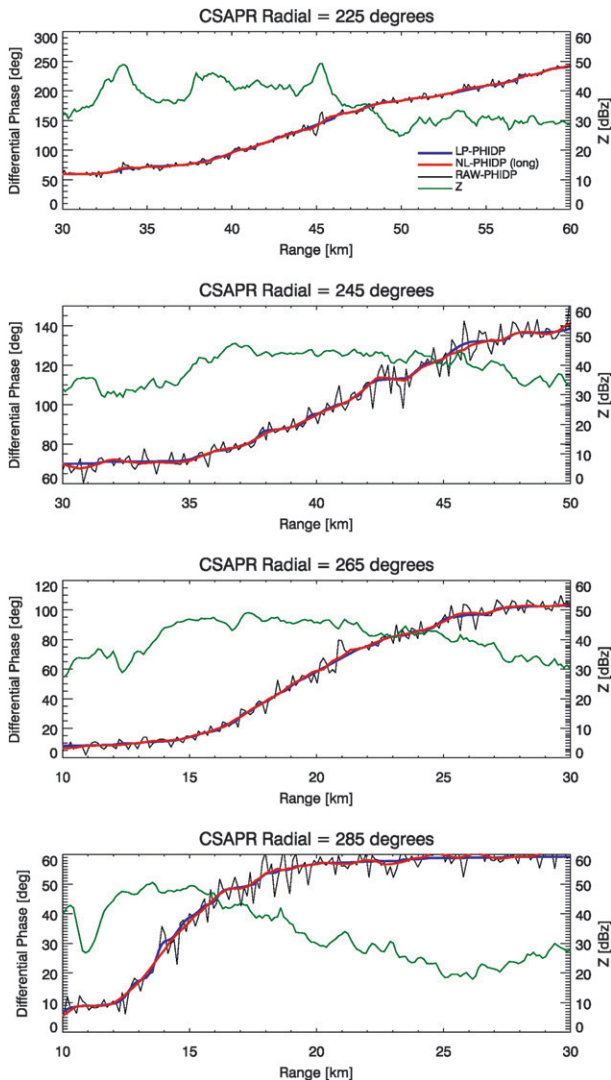


FIG. 8. Select CSAPR radials demonstrating phase-processing behavior and associated  $Z$  fields for the 20 May 2011 event.

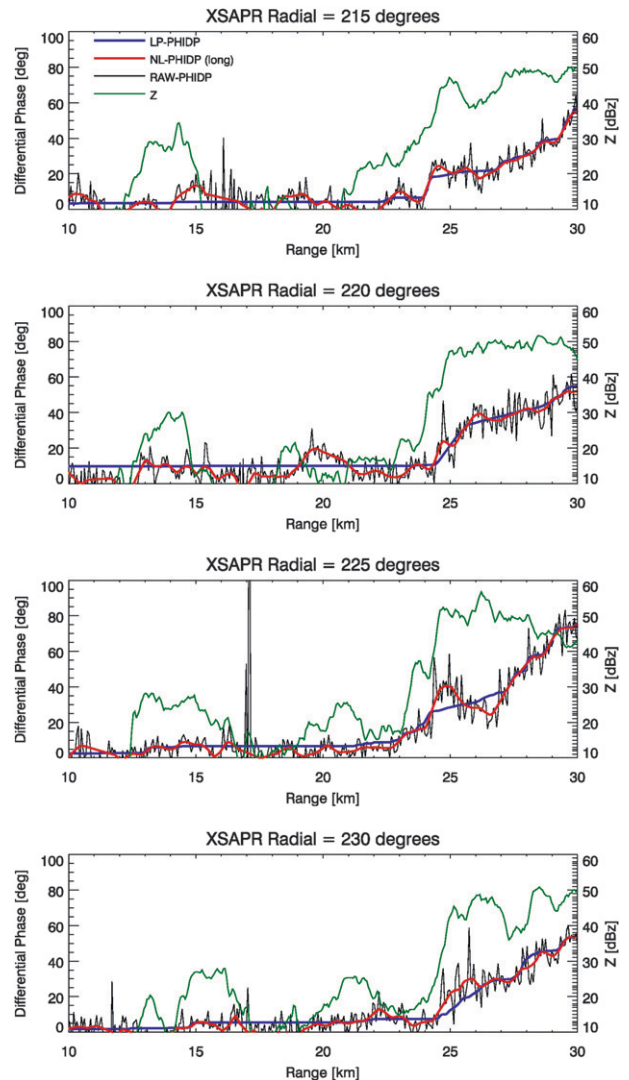


FIG. 9. As in Fig. 8, but for select radials from the 23 May 2011 event of the ARM XSAPR system.

#### 4. Discussion and conclusions

Polarimetric radar differential phase and its range derivative  $K_{DP}$  are of interest to several hydrological applications, including rainfall retrievals and drop size distribution insight. Reducing the uncertainty and unphysical behaviors often found for these fields can have a significant impact on the quality of base polarimetric products of subsequent importance for the forcing of models and/or model evaluation. This study offers a unique approach for differential phase processing that capitalizes on LP ideas and conventional methods for solving LP problems. The apparent success of this method is encouraging for subsequent radar applications and improvements of other physical retrieval problems (radar or otherwise).

Within this study, the LP approach was simple yet designed to replicate many desirable qualities of  $\Phi_{DP}$  and  $K_{DP}$  behaviors sought by other currently available radar processing methods. As compared to standard published methods, the strength of these LP methods is an ability to enforce monotonic behaviors if desired. If the original data array behaves according to the constraint conditions, then there is no requirement that the data be altered (smoothed). Additional constraints, including polarimetric self-consistency, are apparently not difficult to explore in future iterations of these methods. Our simple “bounding” of this phase problem using (typically) more robust  $Z$  field constraints improves the visual appearance of the  $K_{DP}$  fields. As with more complex and/or published nonlinear variational methods, there is ultimately a clear

trade-off between method flexibility when applying realistic constraints and the additional computational expense for LP methods that scales with the number of data and constraint equations. Most computational costs were not found prohibitive for the DOE ARM computing framework, although ARM's emphasis is on algorithm reliability and product quality.

In this LP approach, the monotonicity constraint is always maintained. Specifically, the optimal solution includes a small five-point derivative filter length over which  $K_{DP}$  is nonnegative. This implies that the solution  $\Phi_{DP}$  values at subfilter lengths may still exhibit non-monotonic fluctuation. Yet, these fluctuations can be handled by applying the optimal, offsetting smoothing filter as in section 2 (Figs. 1–3). The nonnegative property of our offered LP approach is not necessarily a behavior that is strongly enforced within other processing schemes. Recent exceptions include a nonlinear variational method wherein this behavior is guaranteed by applying a cost function to be minimized that includes a smoothing (low-pass filter) term with a tunable control parameter (e.g., Maesaka et al. 2012). For many fixed-length smoothing approaches, as is the case with the 9- and 25-gate options utilized in the NSSL method, these may be coupled to provide monotonic behaviors under certain conditions and at the longer wavelengths for which they were originally developed. Yet, Fig. 9 indicates that the current NSSL 25-gate “heavily” smoothed option (approximately 2–3-km window at ARM radars) is not sufficient to guarantee this behavior and that a longer filter (or iterative adjustment) would be required to consistently guarantee this behavior. In this way, even basic LP methods described in this manuscript suggest some benefit, since these methods maintain a small filter length and avoid improper smearing of differential phase data with range to achieve the monotonic behavior.

The Kalman filter approach recently proposed by Schneebeli and Berne (2012) appears quite elegant in design. The presented LP solutions for differential phase processing and improved phase-precipitation “mapping,” however, are not attempting a unified moment or simultaneous holistic polarimetric radar measurement improvement as in that approach. The current LP method descriptions in this study only consider  $Z$  moment behavior (which is corrected for attenuation in rain using linear methods; e.g., Bringi et al. 1990) as weak steering for nonzero  $K_{DP}$  to range gates of enhanced  $Z$ . Nevertheless, a primary concern for a more holistic approach in the Oklahoma ARM environment is the severity of the convective storm regimes (likelihood of hail, NBF) and the associated quality of polarimetric  $Z_{DR}$  measurements at those shorter ARM wavelengths. This tends to argue for capitalizing on “relative” (nonabsolute

calibration) behaviors as a means to incorporate  $Z$  and  $Z_{DR}$  into LP scheme constraints [e.g., adapting constraint ideas as from Otto and Russchenberg (2011)]. However, these are topics of future effort and beyond the scope of the present demonstration of LP methods.

*Acknowledgments.* This paper has been authored by employees of Brookhaven Science Associates, LLC, under Contract DE-AC02-98CH10886 with the U.S. Department of Energy. The publisher by accepting the manuscript for publication acknowledges that the U.S. government retains a nonexclusive, paid-up, irrevocable, worldwide license to publish or reproduce the published form of this manuscript, or allow others to do so, for U.S. government purposes. Doctor Giangrande's work is supported by the Climate Science for a Sustainable Energy Future project of the Earth System Modeling (ESM) program in the DOE Office of Science. Doctor McGraw's support is from the FASTER project (<http://www.bnl.gov/faster/>) supported by the DOE ESM program. The authors thank Drs. Alexander Ryzhkov (OU-NSSL), Michele Galletti (BNL), and Guifu Zhang (OU) for critical discussions throughout the writing process as well as the comments of several anonymous reviewers. Additional ARM radar dataset support and operational implementation were assisted by Dr. Scott Collis (ANL). A version of the LP-based method described by this manuscript and all associated datasets are freely available online (<http://www.arm.gov>) and as part of the open-source Python ARM Radar Toolkit.

## REFERENCES

- Ackerman, T. P., and G. M. Stokes, 2003: The Atmospheric Radiation Measurement Program. *Phys. Today*, **56**, 38–44.
- Bazaraa, M. S., J. J. Jarvis, and H. D. Sherali, 2010: *Linear Programming and Network Flows*. 4th ed. Wiley, 768 pp.
- Bharadwaj, N., V. Chandrasekar, and F. Junyent, 2010: Signal processing system for the CASA Integrated Project I radars. *J. Atmos. Oceanic Technol.*, **27**, 1440–1460.
- Bringi, V. N., and V. Chandrasekar, 2001: *Polarimetric Doppler Weather Radar: Principles and Applications*. Cambridge University Press, 636 pp.
- , —, N. Balakrishnan, and D. S. Zrnić, 1990: An examination of propagation effects in rainfall on radar measurements at microwave frequencies. *J. Atmos. Oceanic Technol.*, **7**, 829–840.
- Cheong, B. L., R. D. Palmer, and M. Xue, 2008: A time series weather radar simulator based on high-resolution atmospheric models. *J. Atmos. Oceanic Technol.*, **25**, 230–243.
- Cifelli, R., V. Chandrasekar, S. Lim, P. C. Kennedy, Y. Wang, and S. A. Rutledge, 2011: A new dual-polarization radar rainfall algorithm: Application in Colorado precipitation events. *J. Atmos. Oceanic Technol.*, **28**, 352–364.
- Dantzig, G. B., 1963: The simplex method. *Linear Programming and Extensions*, Princeton University Press, 94–119.

- Enke, C. G., and T. A. Nieman, 1976: Signal-to-noise ratio enhancement by least-squares polynomial smoothing. *Anal. Chem.*, **48**, 705A–712A.
- Giangrande, S. E., and A. V. Ryzhkov, 2005: Calibration of dual-polarization radar in the presence of partial beam blockage. *J. Atmos. Oceanic Technol.*, **22**, 1156–1166.
- , and —, 2008: Estimation of rainfall based on the results of polarimetric echo classification. *J. Appl. Meteor. Climatol.*, **47**, 2445–2462.
- Goddard, J. W. F., J. Tan, and M. Thurai, 1994: Technique for calibration of meteorological radar using differential phase. *Electron. Lett.*, **30**, 166–167.
- Gourley, J. J., S. E. Giangrande, Y. Hong, Z. L. Flamig, T. Schuur, and J. A. Vrugt, 2010: Impacts of polarimetric radar observations on hydrologic simulation. *J. Hydrometeorol.*, **11**, 781–796.
- Gu, J.-Y., A. Ryzhkov, P. Zhang, P. Neilley, M. Knight, B. Wolf, and D.-I. Lee, 2011: Polarimetric attenuation correction in heavy rain at C band. *J. Appl. Meteor. Climatol.*, **50**, 39–58.
- Helbush, R. E., 1968: Linear programming applied to operational decision making in weather risk situations. *Mon. Wea. Rev.*, **96**, 876–882.
- Hubbert, J., and V. N. Bringi, 1995: An iterative filtering technique for the analysis of copolar differential phase and dual-frequency radar measurements. *J. Atmos. Oceanic Technol.*, **12**, 643–648.
- , V. Chandrasekar, V. N. Bringi, and P. Meischner, 1993: Processing and interpretation of coherent dual-polarized radar measurements. *J. Atmos. Oceanic Technol.*, **10**, 155–164.
- Jung, Y., G. Zhang, and M. Xue, 2008a: Assimilation of simulated polarimetric radar data for a convective storm using the ensemble Kalman filter. Part I: Observation operators for reflectivity and polarimetric variables. *Mon. Wea. Rev.*, **136**, 2228–2245.
- , M. Xue, G. Zhang, and J. M. Straka, 2008b: Assimilation of simulated polarimetric radar data for a convective storm using the ensemble Kalman filter. Part II: Impact of polarimetric data on storm analysis. *Mon. Wea. Rev.*, **136**, 2246–2260.
- Kiountouzis, E. A., 1973: Linear programming techniques in regression analysis. *J. Roy. Stat. Soc.*, **22C**, 69–73.
- Lei, L., G. Zhang, B. L. Cheong, and R. Palmer, 2009: Simulations of polarimetric radar signals based on numerical weather prediction model output. Preprints, *25th Conf. on Int. Interactive Information and Processing Systems for Meteorology, Oceanography, and Hydrology*, Phoenix, AZ, Amer. Meteor. Soc., P2.8. [Available online at [https://ams.confex.com/ams/89annual/techprogram/paper\\_145884.htm](https://ams.confex.com/ams/89annual/techprogram/paper_145884.htm).]
- Madden, H. H., 1978: Comments on the Savitzky-Golay convolution method for least-squares-fit smoothing and differentiation of digital data. *Anal. Chem.*, **50**, 1383–1388.
- Maesaka, T., K. Iwanami, and M. Maki, 2012: Non-negative  $K_{DP}$  estimation by monotone increasing  $\Phi_{DP}$  assumption below melting layer. Preprints, *Seventh European Conf. on Radar in Meteorology and Hydrology*, Toulouse, France, Météo-France, 26 QPE. [Available online at [http://www.meteo.fr/cic/meetings/2012/ERAD/extended\\_abs/QPE\\_233\\_ext\\_abs.pdf](http://www.meteo.fr/cic/meetings/2012/ERAD/extended_abs/QPE_233_ext_abs.pdf).]
- Matrosov, S. Y., R. Cifelli, P. C. Kennedy, S. W. Nesbitt, S. A. Rutledge, V. N. Bringi, and B. E. Martner, 2006: A comparative study of rainfall retrievals based on specific differential phase shifts at X- and S-band radar frequencies. *J. Atmos. Oceanic Technol.*, **23**, 952–963.
- Minciardi, R., R. Sacile, and F. Siccardi, 2003: Optimal planning of a weather radar network. *J. Atmos. Oceanic Technol.*, **20**, 1251–1263.
- Otto, T., and H. W. J. Russchenberg, 2011: Estimation of specific differential phase and differential backscatter phase from polarimetric weather radar measurements of rain. *IEEE Geosci. Remote Sens. Lett.*, **8**, 988–992.
- Park, S. G., M. Maki, K. Iwanami, V. N. Bringi, and V. Chandrasekar, 2005: Correction of radar reflectivity and differential reflectivity for rain attenuation at X band. Part II: Evaluation and application. *J. Atmos. Oceanic Technol.*, **22**, 1633–1655.
- Portnoy, S., and R. Koenker, 1997: The Gaussian hare and the Laplacian tortoise: Computability of squared-error versus absolute-error estimators. *Stat. Sci.*, **12**, 279–300.
- Ray, P. S., B. C. Johnson, K. W. Johnson, J. S. Bradberry, J. J. Stephens, K. K. Wagner, and J. B. Klemp, 1981: The morphology of severe tornadic storms on 20 May 1997. *J. Atmos. Sci.*, **38**, 1643–1663.
- Ryzhkov, A. V., 2007: The impact of beam broadening on the quality of radar polarimetric data. *J. Atmos. Oceanic Technol.*, **24**, 729–744.
- , and D. S. Zrnić, 1998: Beamwidth effects on the differential phase measurements of rain. *J. Atmos. Oceanic Technol.*, **15**, 624–634.
- , S. E. Giangrande, V. M. Melnikov, and T. J. Schuur, 2005a: Calibration issues of dual-polarization radar measurements. *J. Atmos. Oceanic Technol.*, **22**, 1138–1155.
- , —, and T. J. Schuur, 2005b: Rainfall estimation with a polarimetric prototype of WSR-88D. *J. Appl. Meteor.*, **44**, 502–515.
- Scarchilli, G., E. Gorgucci, V. Chandrasekar, and A. Dobaie, 1996: Self-consistency of polarization diversity measurement of rainfall. *IEEE Trans. Geosci. Remote Sens.*, **34**, 22–26.
- Schneebeil, M., and A. Berne, 2012: An extended Kalman filter framework for polarimetric X-band weather radar data processing. *J. Atmos. Oceanic Technol.*, **29**, 711–730.
- Smyth, T. J., and A. J. Illingworth, 1998: Correction for attenuation of radar reflectivity using polarization data. *Quart. J. Roy. Meteor. Soc.*, **124**, 2393–2415.
- Vivekanandan, J., G. Zhang, and M. K. Politovich, 2001: An assessment of droplet size and liquid water content derived from dual-wavelength radar measurements to the application of aircraft icing detection. *J. Atmos. Oceanic Technol.*, **18**, 1787–1798.
- , —, S. M. Ellis, D. Rajopadhyaya, and S. K. Avery, 2003: Radar reflectivity calibration using differential propagation phase measurement. *Radio Sci.*, **38**, 8049, doi:10.1029/2002RS002676.
- Wang, Y., and V. Chandrasekar, 2009: Algorithm for estimation of the specific differential phase. *J. Atmos. Oceanic Technol.*, **26**, 2565–2578.
- , and —, 2010: Quantitative precipitation estimation in the CASA X-band dual-polarization radar network. *J. Atmos. Oceanic Technol.*, **27**, 1665–1676.
- Xue, M., K. K. Droegemeier, and V. Wong, 2000: The Advanced Regional Prediction System (ARPS)—A multiscale nonhydrostatic atmospheric simulation and prediction tool. Part I: Model dynamics and verification. *Meteor. Atmos. Phys.*, **75**, 161–193.
- Zrnić, D. S., and A. Ryzhkov, 1996: Advantages of rain measurements using specific differential phase. *J. Atmos. Oceanic Technol.*, **13**, 454–464.